ELSEVIER

Journal of Nuclear Materials 290–293 (2001) 518–524

journal of nuclear materials

www.elsevier.nl/locate/jnucmat

Section 6. Plasma edge physics and support

Interpretation of SOL flows and target asymmetries in JET using EDGE2D code calculations

A.V. Chankin *, G. Corrigan, S.K. Erents, G.F. Matthews, J. Spence, P.C. Stangeby [1]

EURATOM/UKAEA Fusion Association, Culham Science Centre, Jet Joint Undertaking, Culham, Abingdon, Oxfordshire, OX14 3EA, UK

Abstract

The EDGE2D code with drifts can satisfactorily reproduce measured target asymmetries in the JET field reversal experiments. It also reveals the parallel flow pattern in the main scrape-off layer (SOL) region, which mainly consists of the ion Pfirsch–Schlüter flow and the return parallel flow caused by the poloidal $E_r \times B$ drift. Individual switches for the drifts in the EDGE2D enabled one to separate effects of various drifts. It was found that ∇B and centrifugal drifts cause the largest target asymmetries and SOL flows. However, $E \times B$ drifts were also found to produce the right trends in the asymmetries. © 2001 Published by Elsevier Science B.V.

Keywords: 2D Model; Divertor modelling; SOL plasma

1. Introduction

Inclusion of classical drifts into 2D edge codes is an important step in the scrape-off layer (SOL) and divertor modelling. It provides the clue for understanding changes in the target asymmetries observed in field reversal experiments and the nature of SOL flows. The version of EDGE2D with drifts has been created in view of achieving these goals. Main equations of this code and the results of the attempts to model JET experimental data have been reported in [1–3]. Although only a pure hydrogen/deuterium version of this code has been realised so far (with the radiated power inside the computational grid calculated according to [4]), the code has demonstrated its ability to satisfactorily match experimental target profiles simultaneously for both (normal and reverse) toroidal field (B_t) directions.

Initial results runs of EDGE2D [2] were focused on establishing the role of $E \times B$ drifts in creating target asymmetries. Earlier models and conceptions, developed in the approximation of *cylindrical* geometry, pointed to either of these drifts, poloidal or radial, as being primarily responsible for the target asymmetries [5–11]. At the same time, diamagnetic flows were shown to have no impact on the particle and heat flows [8]. The importance of $E \times B$ drifts, especially in the divertor region, has been confirmed in some other 2D code calculations in divertor geometry [12–16], however, they alone were found to be insufficient to explain target asymmetries in [17]. On the other hand, recent EDGE2D results have brought out the role of the ∇B and centrifugal drifts in creating target asymmetries and SOL flows [3]. To explain these latest results, a fluid model based on the effect of the ion diamagnetic flow on poloidal asymmetries in high recycling SOLs in a simple *toroidal* geometry has been developed [18]. The model predicts a significant effect of $j_r \times B$ forces caused by up–down pressure asymmetry (seen in the EDGE2D output) on the target asymmetries. $j_r \times B$ forces were first proposed as a possible explanation for the generation of the SOL toroidal momentum and target asymmetries in [19] (albeit, in *cylindrical* geometry and neglecting strong local radial currents in the magnetic pre-sheath regions).

* Corresponding author. Permanent address: Russian Scientific Centre 'Kurchatov Institute', Institute for Nuclear Fusion, Kurchatova, sq. 46, Moscow 123182, Russian Federation. Tel.: +44-1235 465 281; fax: +44-1235 464 766.

E-mail address: alexc@jet.uk (A.V. Chankin).

[1] Permanent address: University of Toronto, Institute for Aerospace Studies, Ontario, Canada, M3H 5T6.

0022-3115/01/$ - see front matter © 2001 Published by Elsevier Science B.V.
PII: S0022-3115(00)00516-X

The present paper gives a systematic account of drift effects on target asymmetries and SOL flows as seen in the EDGE2D code. Individual switches for various drifts have been introduced into the code to get a deeper insight into underlying physics of drift effects in the SOL. It was, however, found that blockage of radial currents through the separatrix (in the conditions where ∇B and centrifugal drifts where switched on in the core but switched off in the SOL and vice versa) severely affected numerical stability of calculations and created unphysical boundary conditions for the SOL region. At the same time, no such detrimental effects where observed for $E \times B$ drifts, partly because the divergence of $E \times B$ flows could be compensated by anomalous diffusive particle flows. For that reason, all cases with only $E \times B$ drifts switched on in the SOL were run under conditions where ∇B and centrifugal drifts were also switched off in the core, leaving the core without drifts. At the same time, cases with $E \times B$ drifts switched off in the SOL were run under conditions where ∇B and centrifugal drifts were switched on in the core, alongside over $E \times B$ drifts. Thus, cases where ∇B/centrifugal and $E \times B$ drifts were switched on separately in the SOL were under different conditions in the core (all drifts switched on in the core and all drifts switched off in the core, respectively). This, however, did not affect the plasma core profiles and created similar conditions at the separatrix, since in both limiting cases in the core radial profiles of plasma parameters, including ion toroidal rotation, were the same, with only the radial electric field (E_r) being different.

2. Changes to target profiles introduced by drifts

The main equations used in the drifts implementation into EDGE2D code can be found in [1]. Boundary conditions at the targets, set at the entrance to the magnetic pre-sheath (MPS), have also been modified according to [20]. They account for the poloidal $E \times B$ flow into the MPS, but do not include radial $E \times B$ drifts in the MPS and the sheath. The computational grid used for running EDGE2D cases is shown in Fig. 1. This figure also shows the position of the reciprocating Langmuir probe (RCP) in JET, for easy comparison between the code output and experimental data. The probe has two sides facing ion and electron drift directions and can measure the Mach number of the ion parallel flow. Experimental profiles of the Mach number measured by the probe have been presented elsewhere [21,22] (see also [3] where Mach number profiles were replicated for comparison with EDGE2D output). It has been demonstrated that EDGE2D can satisfactorily reproduce measured target asymmetries and their changes in the JET field reversal experiments [3].

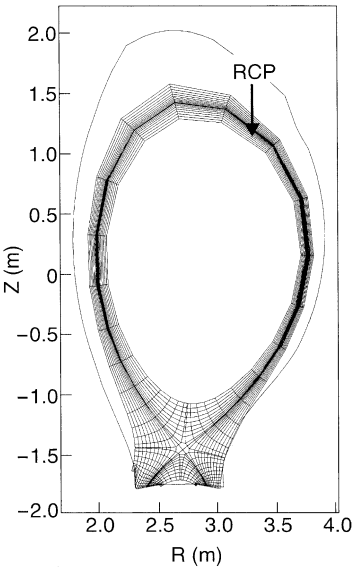

Fig. 1. Computation grid used for EDGE2D cases, with the position of the reciprocating Langmuir probe (RCP) indicated by the arrow.

For detailed analysis of the drifts effects on the target profiles and SOL flows, a case with the 6 MW of input power into the grid, shared equally between ion and electron channels, radiated power of 2 MW and separatrix density $n_e = 1.2 \times 10^{19}$ m^{-3} was selected. Input power was reduced compared with the previously analysed case [3], in order to avoid high ion temperature regime in the SOL where kinetic effects become important. Transport coefficients, constant in the magnetic flux space, were used with values at the midplane: $D_\perp = 0.1$ m^2 s^{-1}, $\chi_e = \chi_i = 0.5$ m^2 s^{-1}, pinch velocities $V_{pinch} = 3$ and 0.5 m s^{-1} in the SOL and core, respectively. Note that heat conductivities were reduced by half compared with the previous case in [3], taking account of lower typical χ_e values extracted from the DIVIMP modelling. All drifts were switched on both in the SOL and in the core for all the results presented in Figs. 2, 3, 5 and 8, unless otherwise specified (as in Figs. 4, 6, and 7).

Fig. 2 presents a plot of the n_e contours in the divertor region for the cases with normal (ion ∇B drift directed towards the target) and reversed (ion ∇B drift directed away from the target) B_t directions. It demonstrates the ability of the code to reproduce the main trend for higher density plasma in the inner divertor leg observed in normal B_t discharges (see, e.g., [23]). Target profiles of n_e, T_e, target electric current density j_{target} and power flux, P_{target}, which includes recombination power, are presented in Fig. 3. Density asymmetries introduced by the drifts are accompanied by T_e asymmetries, with the plasma being much cooler at the inner target in the

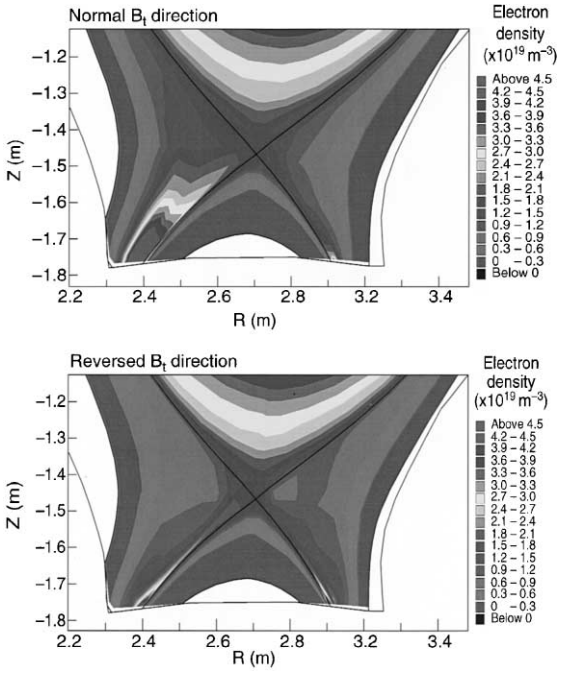

Fig. 2. Electron density contour plots in the divertor region in cases with normal and reversed B_t directions.

normal B_t case, consistent with direct experimental observations [23] and the tendency for earlier plasma detachment from the inner target in normal B_t discharges (see, e.g., [24]). Larger T_e asymmetries cause larger current densities j_{target} in normal B_t case, which are mainly due to the thermoelectric current [25]. Much lower T_e at the inner target in normal B_t case is primarily responsible for extremely large asymmetry of the power at the target, P_{target}. The total power flow, integrated over each target, is 0.53 and 3.01 MW to the inner and outer target, respectively, giving a ratio of 5.7. For the reversed B_t case, the power flows are 1.18 and 2.29 MW, still resulting in the ratio of 1.9 in favour of the outer target.

In order to assess the relative role of $E \times B$ and ∇B/centrifugal drifts in creating target asymmetries, cases were run with only $E \times B$ drifts switched on in the SOL (with all the drifts switched off in the core) and $E \times B$ drifts switched off in the SOL (leaving all the drifts switched on in the core). As was pointed out in Section 1, such an asymmetry between these cases with respect to the situation in the core is necessary to ensure that there is no blockage for the current flow across the separatrix, since in the EDGE2D there is no compensating mechanism for the divergence of radial currents introduced by such blockage (no anomalous radial conductivity). As for the core profiles (except for the radial electric field), they were the same in both cases, providing similar boundary conditions for the SOL. As shown in Fig. 4 for n_e profiles, both $E \times B$ and ∇B/

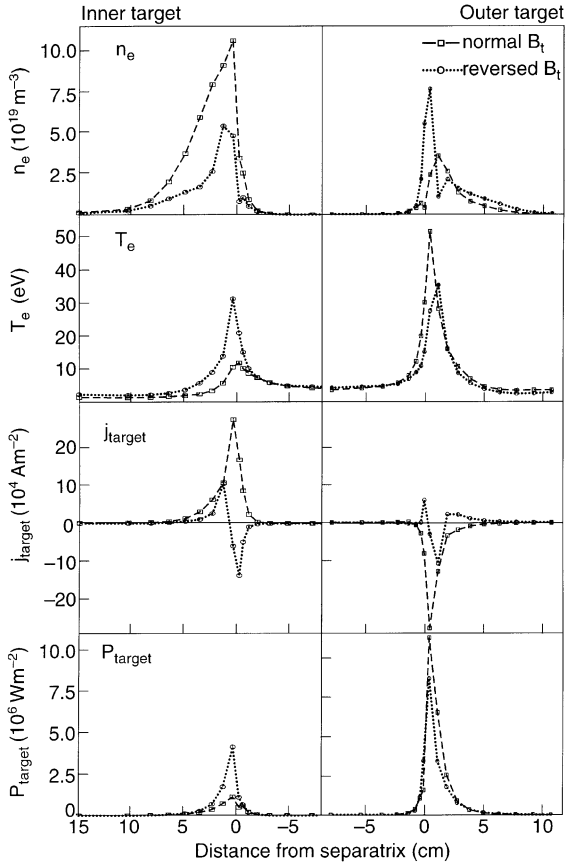

Fig. 3. n_e, T_e, target electric current and power density profiles for normal and reversed B_t cases. Positive values for j_{target} correspond to the current flow into the target.

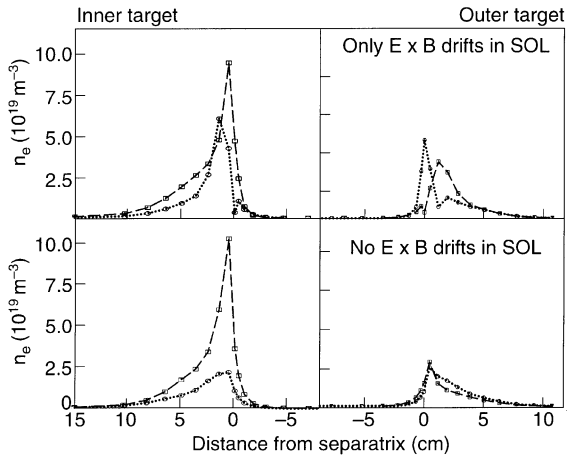

Fig. 4. n_e target profiles in the cases with only $E \times B$ and only ∇B/centrifugal drifts switched on in the SOL, for both B_t directions.

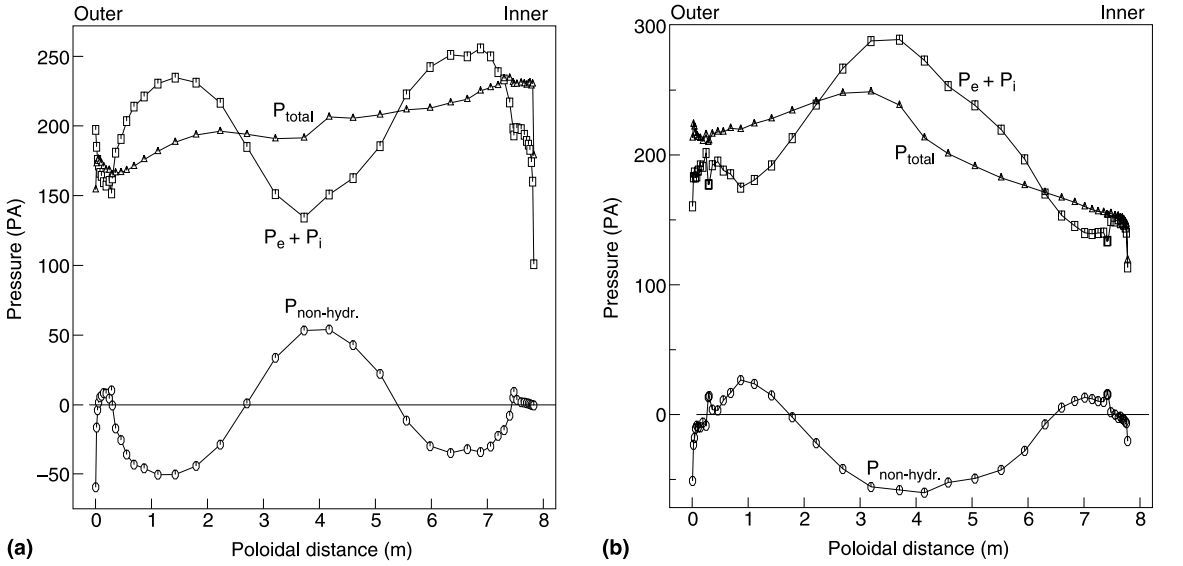

Fig. 5. Poloidal profiles of the ion plus electron static pressure, ion non-hydrostatic (viscous) pressure and total pressure, which also includes ion dynamic pressure, for the third ring outside of the separatrix, marked by the arrow in Fig. 6, for normal (a) and reversed (b) B_t directions.

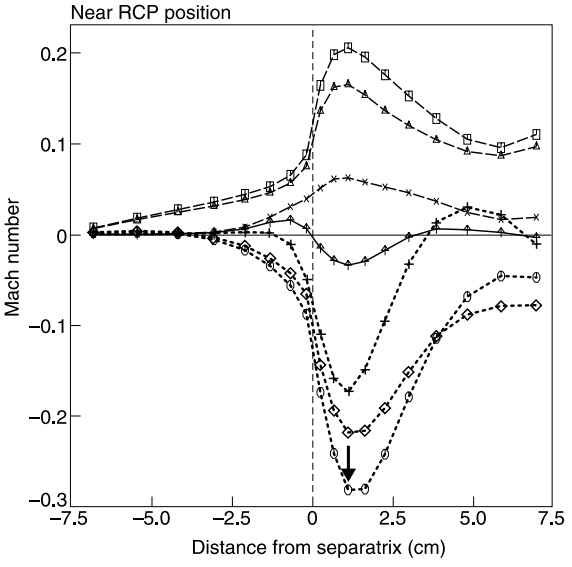

Fig. 6. Radial profiles of the Mach number of the parallel ion flow near the RCP position for different EDGE2D cases. See legend in Fig. 7.

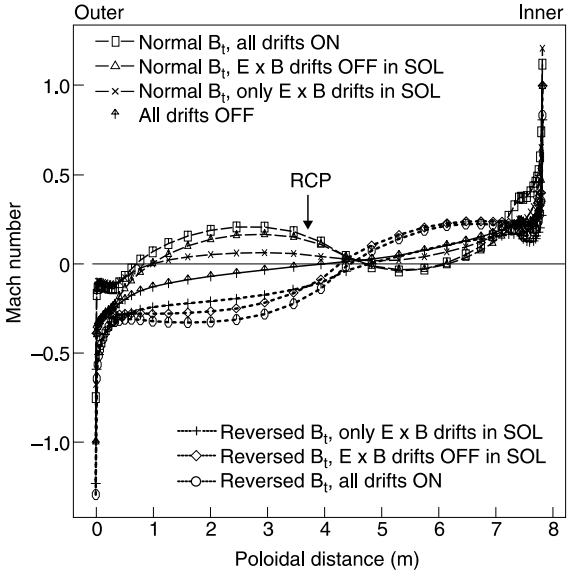

Fig. 7. Poloidal profiles of the Mach number of the parallel ion flow along the third ring outside of the separatrix, marked by the arrow in Fig. 6. Positive SOL parallel ion flow corresponds to the direction from the outer to the inner target.

centrifugal drifts cause changes in target density asymmetries in a qualitative agreement with experimental observations. However, ∇B/centrifugal drifts are more efficient in varying n_e at the inner target. The synergy effect of the two drifts in creating density asymmetries is not observed in these cases. In the modelling, it was not possible to discriminate between the influences of radial and poloidal components of the $E \times B$ drift on the target profiles due to numerical instabilities in the normal B_t case with only the poloidal $E \times B$ drift being switched on in the SOL. The possible origin of dips on the n_e profiles at the outer target introduced by $E \times B$ drifts was found

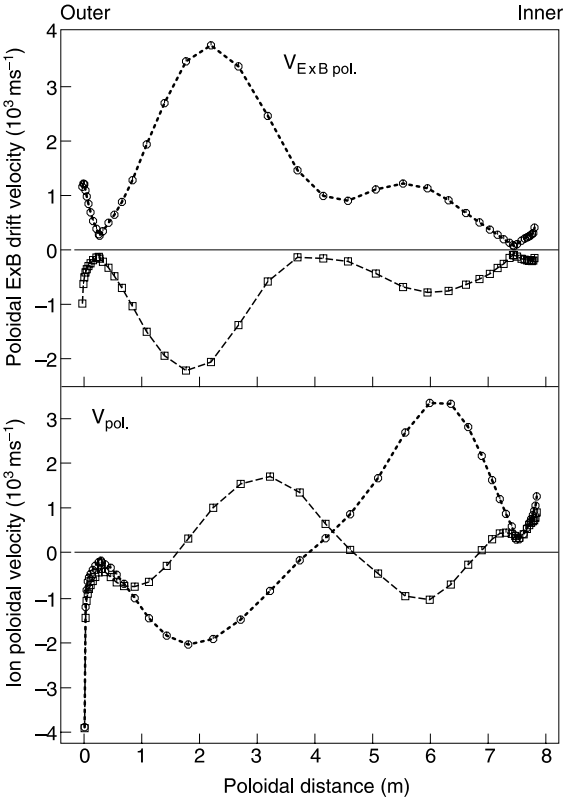

Fig. 8. Poloidal $E \times B$ velocity and ion poloidal velocity (excluding ion diamagnetic flow) along the third ring outside of the separatrix, marked by the arrow in Fig. 6, for the cases with all drifts switched on and both B_t directions.

to be related with the profile of the poloidal electric field across the target, which will be discussed elsewhere.

The origin of the target asymmetries introduced by $E \times B$ drifts was discussed in theoretical papers [6–11,23]. According to [5,7,8,11,23], it is the radial component of the $E \times B$ drift which is responsible for the observed asymmetries. The importance of $E \times B$ flows in the divertor, especially in the private region where radial electric field is large near the separatrix, was emphasised in [12–14] based on the modelling with the UEDGE code, where it was also found that the ∇B drift had a weaker effect on the target asymmetries than $E \times B$ drifts. On the other hand, the role of ∇B/centrifugal drifts was recently highlighted by the EDGE2D results [3], where they were found to be more important than $E \times B$ drifts. The reason for the disagreement between EDGE2D and UEDGE results on the relative role of ∇B/centrifugal and $E \times B$ drifts is unclear. In EDGE2D, ∇B/centrifugal drifts (and, to a lesser extent, $E \times B$ drifts) influence target asymmetries through the net effect of the toroidal/parallel force exerted on the SOL plasma by pressure gradients due to the existence of up–down pressure asymmetries and the toroidal effect of larger area of the outer part of the magnetic surface. The fluid formulation of the problem was developed in [18], where the net toroidal $j_r \times B$ force exerted on the SOL plasma in the toroidal direction of the main plasma current was related to the net current density due to surface-averaging of local diamagnetic currents $j_r = \partial p / E_r B \partial \theta$.

Fig. 5 shows poloidal variation of the static ion plus electron pressure over the poloidal distance for the third ring outside of the separatrix (marked by the arrow in Fig. 6), for the normal (a) and reversed (b) B_t cases. The static pressure is highly up–down asymmetric and is larger at the side towards which ion ∇B drift is directed (at the lower half of the magnetic surface for normal, and upper half – for reversed B_t direction). Also shown in Fig. 5 are the ion non-hydrostatic (viscous) pressure and the total pressure, which includes ion and electron static, ion non-hydrostatic and dynamic pressures, which are all components of the parallel momentum balance equation. Near the X-point, the total pressure is larger at the entrance to the inner divertor than at the entrance to the outer divertor in the normal B_t case. This pressure asymmetry is reversed for the reversed B_t case. In either case, the total pressure is larger at the side representing the ion drift side. In order for such pressure asymmetry between the sides to be sustained, a net parallel/toroidal force exerted on the SOL plasma in the direction of the main plasma current must exist. This force, identified as the net $j_r \times B$ force exerted on the SOL in the fluid formulation of the problem, and the corresponding pressure asymmetries at the entrances to the divertor, are believed to be the main source of target asymmetries [18].

Apart from the steady rise/drop of the total pressure between entrances to the divertor, it shows some variation in the main SOL (especially in the reversed B_t case) which can be attributed to the radial transfer of ion parallel momentum between the rings and sharp drops near the targets due to the plasma–neutral momentum exchange.

3. Flows in the SOL

Radial profiles across the separatrix for the Mach number of the ion parallel flow near the RCP position (for the corner of the mesh shifted outwards from the RCP position in Fig. 1) are shown in Fig. 6 for the above mentioned cases with all drifts switched on, $E \times B$ drifts switched off in the SOL, only $E \times B$ drifts in the SOL, as well as for the no drift case. The Mach numbers are about $M = +0.2$ and $M = -0.3$ for normal and reversed B_t cases, respectively, for the cases where all drifts are switched on. The overall shape of the Mach number profiles agree well with experimental data [21,22]. However, in contrast with the experiment, where the absolute value of the Mach number was greater in normal B_t discharges, EDGE2D predicts slightly larger

M for the reversed B_t case, mainly due to larger E_r in the main SOL region, which causes larger return parallel flow compensating poloidal $E \times B$ drift. A possible explanation of this disagreement is the possibility of a strongly ballooning nature of the anomalous transport which could create extra plasma flows from the outside to the inside, thus adding to the flows in the normal B_t cases and subtracting from the flows in reversed B_t cases. This possibility was checked by creating large in-out asymmetries in particle diffusion coefficient $D_\perp$, but the results did not show any significant changes in the ratio of peak Mach numbers in the two cases with opposite B_t directions. Cases with strongly ballooning heat fluxes have so far suffered from numerical instabilities.

Similar to the situation with target asymmetries, ∇B/centrifugal drifts cause larger parallel flows (in cases with $E \times B$ drifts switched off in the SOL) than $E \times B$ drifts (when they are the only drifts switched on in the SOL). This is related to the fact that in JET experiments and EDGE2D modelled cases the ion diamagnetic flow (which replaces guiding centre ∇B drift in the fluid formulation) is larger than the poloidal $E \times B$ drift. The former originates from the ion pressure gradient and the latter from the radial electric field and both contribute to the velocity of the ion Pfirsch–Schlüter flow [26]:

$$V_{\mathrm{II}}^{\mathrm{PS}} = \frac{2q}{enB} \sin\ \theta \left(enE_r - \frac{\mathrm{d}p_i}{\mathrm{d}r} \right), \tag{1}$$

where poloidal angle θ is counted from the bottom of the torus, counter-clockwise and the sign is correct for normal B_t plasmas, assuming positive velocity directed along the field lines from the outer to the inner target. The ion Pfirsch–Schlüter velocity peaks at the midplane. It was reported to have been detected by the Mach probe positioned below the midplane on JT-60U [27]. In the cases with only ∇B/centrifugal and only $E \times B$ drifts switched on in the SOL, each of the two contributors to the right-hand side of Eq. (1) were in turn effectively switched off. The ion Pfirsch–Schlüter velocity is not the only source of parallel flows in the SOL, since the return parallel flow caused by the poloidal $E \times B$ drift (which is of the order E_r/B_θ) can also contribute to the overall parallel flux pattern (see below).

Poloidal profiles of the Mach number for the above cases are shown in Fig. 7, for the third ring outside of the separatrix, where the parallel flow peaks, marked by the arrow in Fig. 6. For the cases with all drifts switched on one can clearly see that, on top of the poloidally variable, in–out asymmetric ion velocity, which was found to be equal to the Pfirsch–Schlüter velocity given by Eq. (1), there is also a constant shift of the poloidal velocity distribution, corresponding to the existence of the SOL toroidal momentum in the direction of the main plasma current. This results in larger absolute values of the Mach number at the outer midplane than at the inner midplane and the shift in the stagnation point from the top towards the inner side. The toroidal momentum has to be attributed mainly to the return parallel flow caused by the poloidal $E \times B$ drift, as becomes clear from Fig. 8.

The poloidal $E \times B$ drift velocity and the 'total' poloidal velocity, which, however, excludes the ion diamagnetic drift, are plotted in Fig. 8, for the same ring as in Fig. 7. The latter includes the poloidal $E \times B$ flow and poloidal projection of the ion Pfirsch–Schlüter and return parallel flows and can be expressed as

$$V_\theta^{\mathrm{tot}} = -E_r/B + B_\theta/B \times \left(\overline{V}_{\mathrm{II}} + V_{\mathrm{II}}^{PS} \right), \tag{2}$$

where $\overline{V}_{\mathrm{II}}$ denotes surface-averaged, poloidally constant parallel ion velocity. This simplified equation ignores the possibility of the poloidally dependent anomalous particle flux and associated closing parallel flux (however, no such poloidal asymmetry of anomalous fluxes was assumed in the EDGE2D calculations described in this paper). Since the 'total' poloidal velocity, as can be seen from Fig. 8, mainly exhibits poloidally variable ion Pfirsch–Schlüter velocity, one has to conclude that the net poloidal $E \times B$ flow is almost compensated by the poloidal projection of the surface-averaged parallel flow with velocity:

$$\overline{V}_{\mathrm{II}} \approx E_r/B_\theta, \tag{3}$$

This velocity, which determines the SOL toroidal momentum, has the nature of the return parallel flow caused by the poloidal $E \times B$ drift, as was first pointed out in [6]. The net $j_r \times B$ force, therefore, mainly creates target asymmetries rather than accelerates the plasma along the field lines. This is apparently due to high recycling conditions near the targets, which exclude the possibility of any significant net poloidal rotation (apart from the one caused by the ion poloidal diamagnetic flow, which, however, is almost divergence-free) in the main SOL. Similar parallel flow pattern, consisting of the ion Pfirsch–Schlüter and return (closing poloidal $E \times B$ drift) flow, has been obtained in recent modelling with B2.5 code [28,29].

4. Conclusions

The EDGE2D code with drifts can satisfactorily reproduce measured target asymmetries in the JET field reversal experiments. Strong effect of the drifts was observed on both target asymmetries and parallel ion flows. Individual switches for various drifts introduced into the code enabled one to get a deeper insight into the drifts effects on target asymmetries and SOL flows. It was found that ∇B and centrifugal drifts cause the largest target asymmetries and SOL flows. These results are consistent with the predictions of the fluid model based on the influence of the ion diamagnetic flow on

poloidal pressure asymmetries in toroidal geometry, which generate $j_r \times B$ forces [18]. Under typical conditions in the JET SOL, ion diamagnetic flow is considerably larger than the poloidal $E \times B$ flow. However, $E \times B$ drifts (which both radial and poloidal components switched on in the SOL) were also found to produce the right trends in the target asymmetries. The results obtained differ from previous theoretical expectations of the predominant role of $E \times B$ drifts in creating target asymmetries (see, e.g., [23]).

According to the EDGE2D results, parallel flow pattern in the main SOL region mainly consists of the ion Pfirsch–Schlüter flow superimposed on the return parallel flow (of the order E_r/B_θ) caused by the poloidal $E \times B$ drift. This parallel flow is directed from the outer to the inner target in normal B_t plasmas and from the inner to the outer target in reversed B_t plasmas. It is responsible for most of the SOL toroidal momentum. The poloidal projection of this parallel return flow was found to be largely compensated by the poloidal $E \times B$ drift flow. Therefore, EDGE2D does not predict any significant net transfer of ions from one target to the other, with only ion Pfirsch–Schlüter flows affecting local ion poloidal transport.

EDGE2D can also reproduce qualitatively the main feature of the parallel Mach number measurements with the reciprocating probe (RCP) in JET: the reversal of the flow with the B_t reversal. The magnitude of the flow and the shape of the radial profile of the Mach number at the RCP position can roughly be reproduced by the code. Differences remain, however, over the symmetry of the Mach number profiles with the B_t reversal. In the experiment, a shift in the two profiles, implying an extra flow from the outer to the inner target, is observed, which makes the Mach number larger in the normal than in reversed B_t discharges. EDGE2D, on the contrary, predicts rather symmetric profiles, even with slightly larger flows in reversed B_t cases. The reason for this difference between experiment and the code results has not been clarified yet.

Acknowledgements

This work was partly funded by the UK Department of Trade and Industry and EURATOM.

References

[1] G.J. Radford, A.V. Chankin, G. Corrigan, R. Simonini, J. Spence, A. Taroni, Contrib. Plasma Phys. 36 (2/3) (1996) 187.
[2] G.J. Radford, A.V. Chankin, G. Corrigan, R. Simonini, J. Spence, A. Taroni, in: Proceedings of the 24th EPS Conference on Control. Fusion and Plasma Phys., Berchtesgaden., Vol. 21A, Part 1, 9–13 June 1997, p. 125.
[3] A.V. Chankin, J.P. Coad, G. Corrigan, et al., Contrib. Plasma Phys. 40 (2000) 288.
[4] J. Neuhauser, W. Schneider, R. Wunderlich, Nucl. Fusion 26 (1986) 1679.
[5] F.L. Hinton, G.M. Staebler, Nucl. Fusion 29 (1989) 405.
[6] M. Tendler, V. Rozhansky, Comments Plasma Phys. Control. Fusion 13 (1990) 191.
[7] G.M. Staebler, Nucl. Fusion 31 (1991) 729.
[8] A.V. Chankin, P.C. Stangeby, Plasma Phys. Control. Fusion 36 (1994) 1485.
[9] R.H. Cohen, D.D. Ryutov, Comments Plasma Phys. Control. Fusion 16 (1995) 255.
[10] I.H. Hutchinson, B. LaBombard, J.A. Goetz, et al., Plasma. Phys. Control. Fusion 37 (1995) 1389.
[11] P.C. Stangeby, A.V. Chankin, Nucl. Fusion. 36 (1996) 839.
[12] T.D. Rognlien, G.D. Porter, D.D. Ryutov, J. Nucl. Mater. 266–299 (1999) 654.
[13] T.D. Rognlien, D.D. Ryutov, N. Mattor, G.D. Porter, Phys. of Plasmas 6 (1999) 1851.
[14] J.A. Boedo, M.J. Schaffer, R. Maingi, C.J. Lasnier, Phys. Plasmas 7 (2000) 1075.
[15] X. Bonnin, W.L. Rowan, Nucl. Fusion 39 (1999) 1009.
[16] R. Schneider, D. Coster, B. Braams, et al., Contrib. Plasma Phys. 40 (2000) 328.
[17] R. Marchand, M. Simard, Nucl. Fusion 37 (1997) 1009.
[18] A.V. Chankin, P.C. Stangeby, Effect of the Diamagnetic Flow on Poloidal Asymmetries in High Recycling Scrape-off Layers., Nucl. Fusion (submitted).
[19] V. Rozhansky, M. Tendler, Phys. Plasmas 1 (1994) 2711.
[20] P.C. Stangeby, A.V. Chankin, Phys. Plasmas 2 (1995) 707.
[21] S.K. Erents, A.V. Chankin, S.J. Davies, H. Guo, G.F. Matthews, P.J. Harbour, P.C. Stangeby, paper P1.040 presented at 26th EPS Conference on Control Fusion and Plasma Phys., Maastricht., 14–18 June 1999.
[22] S.K. Erents, A.V. Chankin, G.F. Matthews, P.C. Stangeby, Parallel Flow in the JET Scrape-off Layer., Plasma Phys. Control. Fusion (submitted).
[23] A.V. Chankin, J. Nucl. Mater. 241–243 (1997) 199.
[24] A. Loarte, R.D. Monk, J.R. Martín-Solís, et al., Nucl. Fusion 3 (1998) 331.
[25] P.J. Harbour, Contrib. Plasma Phys. 28 4&5 (1988) 417.
[26] J. Hugill, J. Nucl. Mater. 196–198 (1992) 918.
[27] N. Asakura, S. Sakurai, N. Hosogane, M. Shimada, K. Itami, Y. Koide, O. Naito, Nucl. Fusion 39 (1999) 1993.
[28] V. Rozhansky, S. Voskoboynikov, E. Kovaltsova, D. Coster, R. Schneider, Contrib. Plasma Phys. 40 (2000) 423.
[29] V. Rozhansky, S. Voskoboynikov, E. Kovaltsova, D. Coster, R. Schneider, Modelling of Tokamak Edge Plasma for Discharges with Neutral Beam Injection, this conference.